

Observation of emission from chaotic lasing modes in deformed microspheres: displacement by the stable orbit modes

Seongsik Chang*, Jens U. Nöckel†, Richard K. Chang*, and A. Douglas Stone*

* Department of Applied Physics, Yale University, New Haven, Connecticut 06520

† Max-Planck-Institut für Physik komplexer Systeme, Dresden, Germany D-01187

(November 11, 2018)

By combining detailed imaging measurements at different tilt angles with simulations of ray emission from prolate deformed lasing micro-droplets, we conclude that the probability density for the lasing modes in a three-dimensional dielectric microcavity must reside in the chaotic region of the ray phase space. In particular, maximum emission from such chaotic lasing modes is not from tangent rays emerging from the highest curvature part of the rim. The laser emission is observed and calculated to be non-tangent and displaced from the highest curvature due to the presence of stable orbits. In this Letter we present the first experimental evidence for this phenomenon of “dynamical eclipsing”.

42.55.Sa, 05.45.Mt, 42.15.-i, 42.25.-p

Both the Schrödinger equation and the wave equation of optics share the property that their short wavelength limit corresponds to a Hamiltonian dynamics: classical Newtonian mechanics in the former case and ray-optics in the latter. When that dynamics is non-integrable, relating properties of the wave solutions to the classical dynamics is very difficult and has been an area of intense study under the rubric *quantum/wave chaos* [1]. Of particular interest recently is the generic non-integrable case of a mixed phase space in which chaotic and regular regions coexist. It was noted [2–6] by several of the authors that an interesting problem in optics, the resonance and emission properties of deformed spherical and cylindrical dielectric resonators, was just such a problem in wave chaos theory with a mixed phase space, with resonant modes corresponding to both regular and chaotic regions of phase space. It was predicted [3,5,6] that in a substantial parameter range deformed micro-cylinder and micro-spherical lasers would actually lase on a certain type of chaotic mode which we refer to as “chaotic whispering gallery modes” (CWGMs). In this Letter, we report for the first time laser emission patterns unique to the CWGM of deformed micro-droplet lasers. The laser emission from CWGMs is found to be non-tangent and its emission location is displaced from the points of highest curvature where most of the laser emission from regular whispering gallery modes occurs.

Whispering gallery modes (WGMs) are solutions of the wave equation which classically correspond to rays circulating around the boundary reflecting at high angle of incidence; in the dielectric resonator such modes have

long lifetimes due to quasi-total internal reflection at the curved boundary. If angular momentum is conserved, then a metastable well is formed by the centrifugal barrier and the dielectric/air interface; quasi-bound states within this well decay only by tunneling (evanescent leakage) [7]. If the dielectric is deformed, angular momentum is no longer conserved and such a state may emit “over the barrier” by refraction, a “classically allowed” process. Light emission via refraction is non-tangent to the interface, whereas that via tunneling is always tangential. Our observation of spatially displaced non-tangent laser emission is a signature of new types of lasing modes in this system unique to the deformed case.

A CWGM is a solution of the wave equation corresponding to an ensemble of rays in a chaotic region of phase space; and the lifetime of such modes is, for large enough deformation, limited by refractive escape [6]. For a deformed cylindrical resonator, such a mode obtained by exact numerical solution of the wave equation, is depicted in Fig. 1(a). Superimposed on a surface of section (SOS) of the phase space for ray motion, we show the Husimi function of the mode [8], which is a projection of the exact wave solution for a resonant mode onto this SOS. As can be seen in Fig. 1(a), the mode is localized away from the critical angle for total internal reflection, χ_c , but its tail leaks downwards to χ_c in a highly anisotropic fashion, leading to directional emission [4,6] [see the inset of Fig 1(a)]. Previous work analyzed anisotropic emission patterns from deformed lasing droplets [3] and dye jets [4] and found results consistent with, but not unique to, lasing from chaotic modes. Rather recently, deformed cylindrical semiconductor lasers [9] were found to exhibit highly directional and high-power output, but feedback was provided by a mode associated with a non-chaotic “bow-tie” orbit.

The main problem with interpreting observations from microlasers with deformed resonators is that highly directional emission may also be obtained with non-chaotic ray dynamics such as an elliptically-deformed cylinder [see Fig. 1(b)]. It is thus desirable to find a distinct signature of lasing from chaotic modes. One such signature [4,6] is illustrated by the SOS in Figs. 1(a) and 1(b). In the SOS of Fig. 1(a), the islands which represent orbits near stable periodic paths prevent the entry of ray flux from the chaotic regions (neglecting weak tunneling effects). This effect can *displace* the rays of such a chaotic mode from the points of highest curvature at

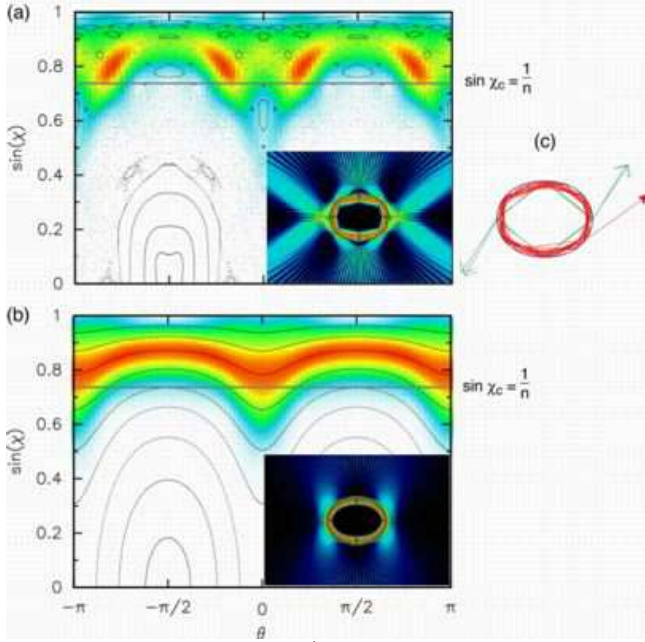


FIG. 1. Husimi plots (red: high intensity, white: no weight) superimposed onto classical surfaces of section for the ray dynamics inside 2D deformed dielectric cavities with refractive index $n = 1.36$. (a) CWGM at $ka = 52.85$ in a quadrupolar cavity parametrized by $r(\theta) = 1 + \epsilon \cos 2\theta$ with $\epsilon = 0.113$. (b) WGM at $ka = 52.04$ in an ellipse with $b/a = 1.27$. Insets: the corresponding wave functions in real space. (c) Sketch of quasi-periodic four-bounce orbits (green) and a chaotic orbit (red) inside the quadrupolar cavity of (a).

which generically high emission would be expected to occur. We refer to the scenario of Fig.1(a) as *dynamical eclipsing*. This displacement of the chaotic mode rays also has a dramatic effect on the laser emission pattern, which can be determined experimentally by taking images of the microcavity at various angles.

The identical ray dynamics underlying Fig. 1(a) for a two-dimensional (2D) microstructure also occurs in a plane that cuts an axisymmetric quadrupole-deformed droplet from pole to pole through a meridian (polar plane). Such droplets made of ethanol (refractive index, $n = 1.36$) containing laser dye are ejected from the vibrating orifice of a Berglund-Liu droplet generator [10], oscillating in shape [3]. The dominant multipole components of this hydrodynamic oscillation [11] are quadrupolar and octupolar with damping time constants $\tau = 213 \mu\text{sec}$ for the quadrupole and $\tau = 39 \mu\text{sec}$ for the octupole. For times $t > 100 \mu\text{sec}$ during which the experiments were performed, the shape deformation is essentially purely quadrupolar, and is uniquely parameterized by the aspect ratio, b/a , where b and a are the semimajor and -minor axes. A particular b/a can be selected by observing the droplets stroboscopically at the proper phase of their shape oscillation.

To detect dynamical eclipsing in the polar plane of such deformed droplets it is necessary to measure both emis-

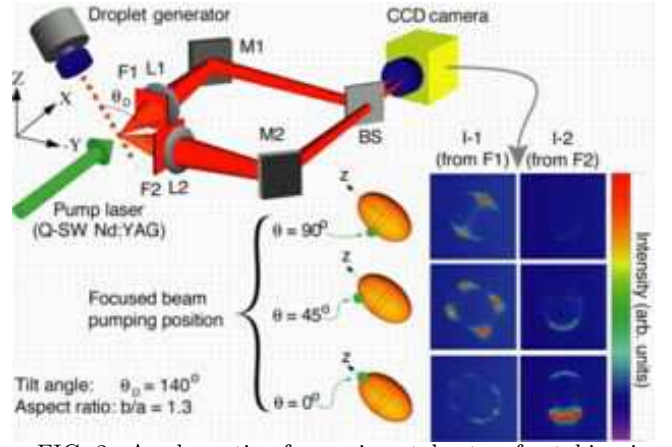


FIG. 2. A schematic of experimental setup for taking images of lasing micro-droplets at various inclination angles (θ_D). (L1, L2: camera lenses; F1, F2: color filters; M1, M2: mirrors; BS: beam splitter). Color filters were used to block scattered pump laser light. Focused pumping with $< 5 \mu\text{m}$ beam diameter was used for the experiment. Images (I-1 and I-2) of prolate droplet ($b/a = 1.3$) at $\theta_D = 140^\circ$ are shown for three different locations of the focused pump beam; (i) equatorial rim, (ii) 45° above the equator, and (iii) north pole.

sion directions and locations on the spheroid. The lasing microdroplets are viewed at various polar angles (θ_D) by using a CCD camera. 2D imaging is essential to determine the emission locations, which cannot be provided by a single-photodiode experiment. The experimental setup is shown in Fig. 2 where the polar plane is defined to be the Y-Z plane. Variation of the polar angle θ_D of the imaging direction is achieved by fixing the camera, but tilting the droplet generator about the pump laser direction (X-axis), which preserves the same (non-uniform) pumping condition at all tilt angles. Simultaneous images were taken in two directions: (I-1) along the X-axis and (I-2) along the (-Y)-axis, which were then brought side by side with a beam splitter (BS) to the single CCD camera. While the shape and the tilt of the droplets were monitored by (I-1), the desired lasing images at various values of θ_D are obtained from (I-2).

We only present data for prolate droplets, for which the longest axis goes through the poles; similar effects are seen in oblate droplets but are not presented here due to space limitations. Taking the long axis as the z-axis, rotational symmetry implies that ray orbits can be classified by the conserved z-component of the *angular momentum*, L_z [3]. The *near-polar orbits* of interest correspond to $L_z \approx 0$, since they correspond to motion in a plane passing near or through the z-axis. Experimentally, lasing in a particular L_z -mode can be excited by aiming a tightly focused pump laser beam along the droplet rim as shown in Fig 2, which subsequently enters the droplet with $\chi \approx \chi_c$ and fixes L_z to a value of $r \sin \theta \sin \chi_c$, where $r(\theta)$ is the distance from the droplet center to the surface (L_z in these units is equal to the

distance of closest approach of the rays to the z axis [3]). Because L_z of such a pump beam is conserved after entering the droplet, this input beam generates the highest gain for lasing modes with the same L_z . For example (see Fig. 2), when pumped at the equatorial rim, lasing occurs in modes with $L_z \approx a \sin \chi_c$ in which rays are confined to the equatorial plane; when pumped tangentially near $\theta = 45^\circ$, lasing occurs in $L_z \approx 0.5a$ modes for which rays precess [12] around the z -axis due to non-zero torque exerted on the rays at each bounce. In the $L_z = 0.5a$ case, the lasing mode is still regular and rays encounter highest curvature near the highest ($\theta = 45^\circ$) or lowest ($\theta = 135^\circ$) latitudes of the orbits and thus escape tangentially through tunneling at these points [13].

In order to demonstrate dynamical eclipsing, near-polar modes ($L_z \approx 0$) are excited with a focused pump beam aimed at the north pole. In this case the ray motion is that of an effective 2D cavity of aspect ratio $b/a \approx 1.3$ formed by the intersection of the droplet with the polar plane, and is identical to the parameters used in Fig. 1(a). No laser emission is observed in I-1, but intense laser emission is observed from the bottom of I-2 (see Fig. 2). Such an emission pattern indicates that main lasing emission does not occur from the highest curvature points (north pole or south pole), but away from these points, consistent with the prediction of dynamical eclipsing in Fig 1(a). To explain this in more detail, note first that there exists a four-bounce stable diamond-shaped orbit for rays in the polar plane [Fig. 1(c)], which can support stable resonant modes; however these modes do not provide sufficient feedback for lasing because of the large refractive leakage near the pole. Specifically, the round-trip loss for the four-bounce orbit is 4.6, which is significantly greater than the estimated maximum round-trip gain of 0.9 for 5×10^{-4} M Rhodamine B dye solution in ethanol. However, chaotic orbits launched with $\chi \gg \chi_c$ can undergo multiple (more than 100) reflections before they reach χ_c . Therefore, the leakage loss of a CWGM is much less than the round-trip gain, and consequently, lasing can occur with feedback provided by chaotic modes. However, the non-lasing four-bounce stable diamond orbits *displace* the laser emission location of the CWGMs [see Fig. 1(a), (c)]. Regular WGMs with $\chi \approx 90^\circ$ still exist for $L_z \approx 0$ and lase for this deformation; however their leakage rate is much smaller than the absorption rate. The fact that the north and south pole is dark indicates the emission from such regular WGM is at least two orders of magnitude weaker than that from dynamically eclipsed CWGM for $L_z \approx 0$.

Figure 3 shows additional results consistent with this interpretation of dynamical eclipsing of CWGMs; in this case an unfocused beam was used to excite all the possible L_z -modes. For the experimental images at $\theta_D = 90^\circ$, the bright regions along the droplet rim are due to a superposition of laser emission from precessing modes at different L_z . The abrupt disappearance of emission at

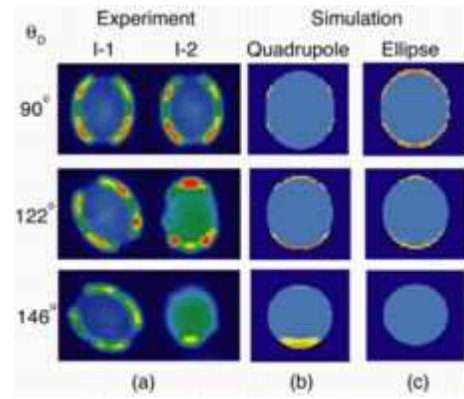


FIG. 3. (a) Experimental lasing images (I-1 and I-2) of broadly-pumped (beam diameter: $> 100 \mu\text{m}$) prolate droplets ($b/a = 1.29$) are shown for $\theta_D = 90^\circ$, 122° , and 146° (pump laser was vertically polarized and f/16 lens was used). Corresponding calculated lasing images (I-2) at $\theta_D = 90^\circ$, 120° , and 150° are shown for quadrupole (b) and elliptic (c) deformations. In the simulation, equally mixed TE and TM polarizations were used to calculate Fresnel coefficients for the emerging laser rays.

the rim near the two poles indicates the absence [3] of such regular precessing modes with $\chi \approx \chi_c$ near $L_z = 0$. A very different emission pattern is seen in I-2 at tilt angles of $\theta_D = 122^\circ$ and 146° ; here we see substantial emission in the plane bisecting the poles of the droplet along the imaging direction; such emission can only come from $L_z \approx 0$ orbits. Moreover the fact that the $L_z \approx 0$ emission is not seen at $\theta_D = 90^\circ$ insures that the emission does not come from the poles (the points of highest curvature), but displaced from the two poles in a manner consistent with the dynamical eclipsing scenario.

Ray simulations of refractive emission for the unfocused pumping case were performed for the quadrupole shape [Fig. 3(b)] and ellipsoid [Fig. 3(c)]. Uniformly distributed rays in θ and L_z were launched with initial χ greater than χ_c . The lasing condition was imposed in the ray simulations by including only orbits which have pathlength (before refractive escape) greater than $1/g$, where the gain is estimated to be $g \approx 45 \text{ cm}^{-1}$. Ray escape was determined by Snell's law and the relevant Fresnel coefficients at each reflection. Note that in the quadrupole simulations, there is strong emission near the bottom center of the image at $\theta_D = 146^\circ$ and no emission at the poles of the image at $\theta_D = 90^\circ$, in good qualitative agreement with the experiments [14]. In contrast, the ellipsoid simulation shows that most of the refractive emission occurs at $\theta_D = 90^\circ$, and essentially no emission is found at $\theta_D = 146^\circ$ in distinct contrast with our experimental results. This result provides crucial support for our interpretation of the images as arising from dynamical eclipsing. The ray motion in the ellipsoid is completely regular, with no chaotic regions and no four-bounce stable islands [see Fig. 1(b)]; hence dynamical

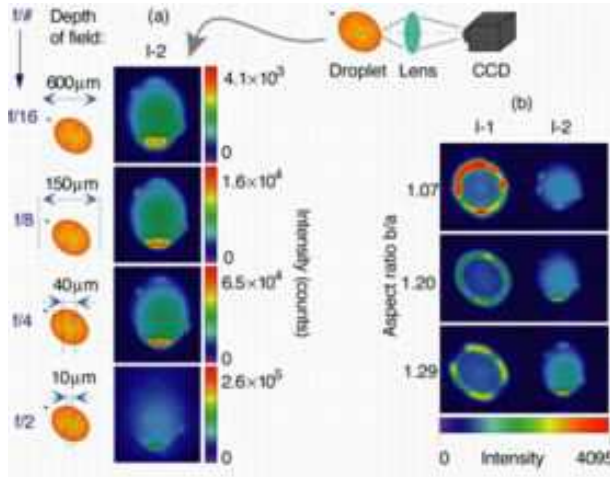


FIG. 4. (a) Images of broadly-pumped lasing prolate droplets ($b/a = 1.29$) at $\theta_D = 142^\circ$ with various f-numbers ($f/16$, $f/8$, $f/4$, and $f/2$). Because the solid angle of light acceptance is proportional to $\approx 1/(f/\#)^2$, the color intensity scale for each $f/\#$ is adjusted accordingly. The depth of field [$\propto (f/\#)^2$] for each $f/\#$ is shown relative to the droplet size. The imaging direction is on the right of the droplet. (b) Lasing images of broadly-pumped prolate droplets with various aspect ratios. Dynamical eclipsing is not present for small deformation ($b/a = 1.07$).

eclipsing does not occur and one finds only tangent emission from the poles [Fig. 1(b), inset].

To further confirm that the emission seen at large tilt angles is non-tangent and hence refractive as we expect from CWGMs, we have varied the depth of field, $d_{f/\#}$, and the acceptance angle (f-number) of the imaging system. In Fig 4(a), images are shown with various $d_{f/\#}$'s for a lasing prolate droplets with $b/a = 1.29$ at $\theta_D = 142^\circ$. The f-number of the camera lens was changed from $f/2$ ($d_{f/2} = 10$ mm, 14% of the droplet size along the imaging axis) to $f/16$ ($d_{f/16} = 600 \mu\text{m}$, covering the whole droplet). While the bright emission is sharply imaged at the bottom center of the image with $f/16$, $f/8$, and $f/4$, the corresponding emission is blurred with $f/2$. From this we conclude that this laser emission is emitted from outside of the region defined by $d_{f/2}$. If such emission propagates parallel to the imaging axis, the emitted rays are non-tangent. For the $f/16$ image, the emission direction is restricted to within 2° from the imaging axis. Laser emission from the displaced location implied by the $d_{f/\#}$ analysis above is non-tangent by as much as $10^\circ - 30^\circ$. Therefore, dynamically eclipsed rays from CWGM are non-tangent up to 30° , which indicates refraction is the major escape mechanism.

Further confirmation comes from the aspect-ratio dependence of the patterns [Fig. 4(b)]. For moderate deformations the islands become too small to generate dynamical eclipsing, and the expected emission from the polar orbits is tangential to the poles as in the case for

the ellipse [see the inset of Fig. 1(b)]. In Fig. 4(b), lasing images at $\theta_D = 142^\circ$ are shown for various b/a ; 1.07, 1.20, and 1.29. For $b/a = 1.07$, the entire rim of the droplet up to the poles is bright in I-1, while no laser emission is recorded in I-2 [note the similarity to the ellipsoid simulations in Fig. 3(c)]. Thus we find a range of intermediate deformations with highly anisotropic emission, but no dynamical eclipsing, which is then turned on by increasing b/a .

In summary, laser emission from a quadrupole-deformed spherical microcavity is observed to be partially non-tangent and displaced from the highest curvature regions. This provides for the first time conclusive evidence of lasing supported by chaotic whispering gallery modes. These modes are displaced from the high curvature points by stable high-loss modes, an effect known as dynamical eclipsing. The unique angular dependence of the lasing images is in good agreement with simulated images of lasing quadrupolar droplets with chaotic ray dynamics.

We would like to acknowledge the partial support of NSF (Grant PHY-9612200).

-
- [1] M. C. Gutzwiller, *Chaos in Classical and Quantum Mechanics* (Springer-Verlag, New York, 1990).
 - [2] J. U. Nöckel, A. D. Stone, and R. K. Chang, *Opt. Lett.* **19**, 1693 (1994).
 - [3] A. Mekis, J. U. Nöckel, G. Chen, A. D. Stone, and R. K. Chang, *Phys. Rev. Lett.* **75**, 2682 (1995).
 - [4] J. U. Nöckel, A. D. Stone, G. Chen, H. Grossman, and R. K. Chang, *Opt. Lett.* **21**, 1609 (1996).
 - [5] J. U. Nöckel, and A. D. Stone, Chapter 11, in *Optical Processes in Microcavities*, edited by R. K. Chang, and A. J. Campillo (World Scientific, Singapore, 1996).
 - [6] J. U. Nöckel and A. D. Stone, *Nature* **385**, 45 (1997).
 - [7] B. R. Johnson, *J. Opt. Soc. Am.* **A10**, 343 (1993).
 - [8] P. LeBoeuf and M. Saraceno, *J. Phys. A Math. Gen.* **23**, 1745 (1990).
 - [9] C. Gmachl, F. Capasso, E. E. Narimanov, J. U. Nöckel, A. D. Stone, J. Faist, D. L. Sivco, and A. Y. Cho, *Science* **280**, 1556 (1998).
 - [10] R. N. Berglund and B. Y. H. Liu, *Envir. Sci. Technol.* **7**, 147 (1973).
 - [11] H. Lamb, *Hydrodynamics* (Dover, New York, 1945) pp. 473-475.
 - [12] J. C. Swindal, D. H. Leach, R. K. Chang, and K. Young, *Opt. Lett.* **18**, 191 (1993).
 - [13] S. Chang, N. B. Rex, and R. K. Chang, *to be published in J. Opt. Soc. Am. B*.
 - [14] Because the ray simulations do not include tunneling, they cannot account for the bright rims in the experimental images at $\theta_D = 90^\circ$.